CHALMERS

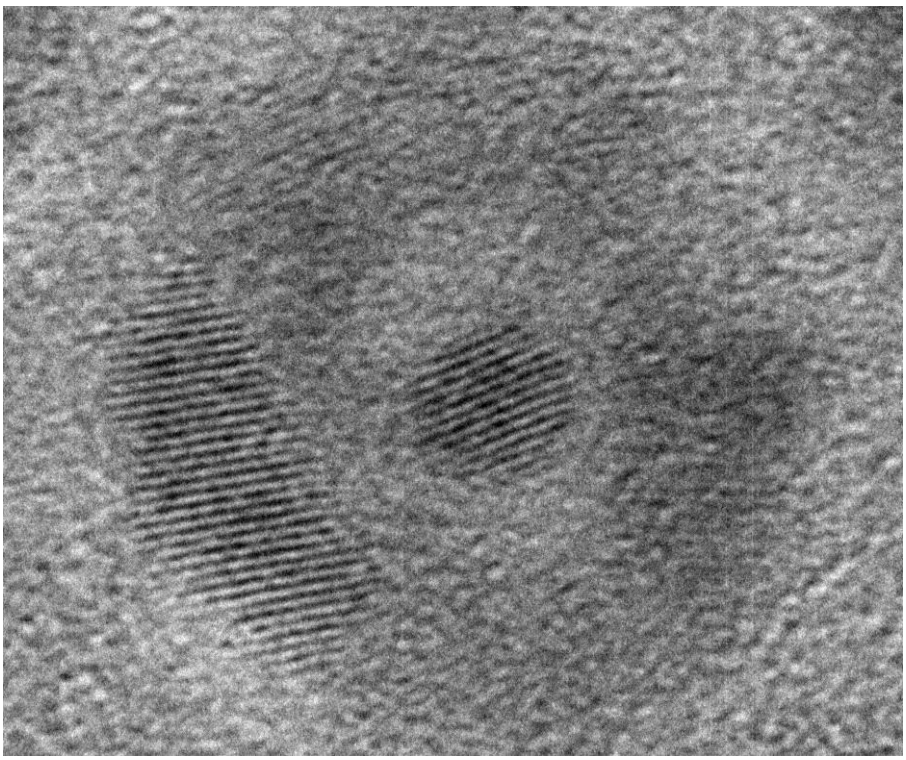

Oxidation of Cobalt Nanocrystals: Investigation of the Role of Nanocrystallinity, Self-Ordering and Nanocrystal Size

Master of Science Thesis in the Master Degree Program, Materials Chemistry and Nanotechnology

JOHANNA BERGSTRÖM

Department of Chemical and Biological Engineering
Division of Applied Chemistry
CHALMERS UNIVERSITY OF TECHNOLOGY
Göteborg, Sweden 2013

Oxidation of Cobalt Nanocrystals: Investigation of the Role of Nanocrystallinity, Self-Ordering and Nanocrystal Size

JOHANNA BERGSTRÖM

The thesis work was performed at Université Pierre et Marie Curie (UPMC) in Paris, France in the Laboratoire des Matériaux Mésoscopiques et Nanométriques and as a part of the SupraNano project group. The project group is directed by Professor Marie-Paule Pileni.

Department of Chemical and Biological Engineering
CHALMERS UNIVERSITY OF TECHNOLOGY
Göteborg, Sweden 2013

Oxidation of Cobalt Nanocrystals: Investigation of the Role of Nanocrystallinity, Self-Ordering and Nanocrystal Size

JOHANNA BERGSTRÖM

Department of Chemical and Biological Engineering
Chalmers University of Technology
SE-412 96 Göteborg
Sweden
Telephone + 46 (0)31-772 1000

Cover:
HRTEM images from polycrystalline fcc nanocrystals produced from organometallic synthesis. One of the obtained structures after oxidation at 200˚C for 10 min, yolk/shell fcc-Co/CoO particle showing the lattice planes for the fcc-Co core and the CoO shell. See page 14 for more information.

Göteborg, Sweden 2013

Acknowledgements

I would like to thank Professor Marie-Paule Pileni for taking me into her group at Laboratoire des Matériaux Mésoscopiques et Nanométriques, at UPMC in Paris. Thank you also to Zhijie Yang and Dr. Jianhui Yang for valuable help and for answering all of my questions and thank you Professor Krister Holmberg for putting me in contact with Professor Pileni and for valuable help from Sweden.

Abstract

The use of cobalt and cobalt oxide nanocrystals has proven promising in technical applications such as information storage, catalysis and Li-ion batteries. Hollow cobalt oxide nanocrystals can be obtained by using the nanoscale Kirkendall effect and the ability to tune the physical properties has made research regarding size, shape, crystal structure and composition into a popular field. However, the effect of the nanocrystallinity on ordered nanoparticles exposed to oxidation has not been considered this extensively in previous research. The effect of nanocrystallinity has been carried out using four different samples, all 8 nm before oxidation, of cobalt nanocrystals synthesized by two different routes, the reverse micelle route for the samples small domain polycrystals and single domain hcp nanocrystals. Synthesized by the second route, the organometallic synthesis, were the other two samples, polycrystalline fcc nanocrystals and single domain ε nanocrystals. The samples were exposed to an oxygen flow for 10 minutes during heating at 200°C or 260°C after which the nanocrystals were characterized using TEM, HRTEM and ED. An investigation of how size affects the oxidation behavior was carried out by using 4, 6 and 8 nm samples from the reverse micelle route. Poly- and single domain crystal Co-nanoparticles showed different oxidation behavior. Single crystalline Co-nanoparticles have a higher tendency to form hollow nanoparticles than polycrystalline Co-nanoparticles. The difference in oxidation behavior is also clear between the two single crystalline and between the two poly crystalline structures. Isolated nanocrystals have a higher probability of being fully oxidized than ordered nanocrystals and the size of the nanocrystals as well as the oxidation temperature has an effect on which oxide, the cubic CoO or the spinal Co_3O_4, is obtained after oxidation.

Keywords: Co nanoparticles, nanocrystallinity, 2D ordering effect, nanocrystal size effect, core/shell structures, hollow structures, yolk/shell structures.

Table of Contents

1. Introduction

Metal oxides are commonly used today in a variety of applications from cathodes in batteries to semiconductors in solar cells (1), (2). Hollow inorganic nanocrystals possess the interesting phenomena of having an empty internal space which creates possibilities for usage in optical, catalytically and magnetic devices such as nanoreactors and carriers for drug delivery (3). The ability to tune physical properties of metal oxides nanoparticles has done the investigation regarding size, shape, crystal structure and composition into a popular field (4), (3). However, not as much attention has been focused on how the crystallinity of the nanoparticle, called the nanocrystallinity, affects the physical properties (4), (5).

Magnetic transition metals, like cobalt (Co), are often air sensitive which makes them complicated to work with. As a consequence of this, metal oxides are used in magnetic applications instead despite the weaker magnetic properties, as they are stable in an air containing environment (6). Co and cobalt oxides (CoO, Co_3O_4) are promising materials when it comes to usage in technical applications such as catalysis, information storage and Li-ion batteries (7). CoO hollow nanocrystals can be successfully synthesize by the Kirkendall effect starting from solid Co nanoparticles and exposing them to a flow of oxygen (8). The Kirkendall phenomenon of diffusion arises during heating when two species in a diffusion couple have different atomic diffusivities (9). As an effect, pores will form in the faster diffusing material, because of a motion of the boundary layer, and can be supersaturated to form a single interior void or a yolk-shell structure (8), (10). Diffusion is made easier by defects in the lattice, like grain boundaries, since this enables atomic jumps. A hollow core formation can be prevented by the produced phase being rich in defects which can absorb the vacancies without forming voids or by the particle being too small to be stable as a hollow structure (11). The synthesis of hollow nanocrystals through the Kirkendall effect provides a template free route which automatically eliminates the sometimes difficult step of removing the template before obtaining the hollow particle (3).

It has been shown that the nanocrystallinity of isolated 7 nm Cobalt nanocrystals does not play a role for oxidation, as they are completely oxidized independently of their nanocrystallinity. As the particles are assembled into a compact hexagonal network in a 2D lattice, the oxygen diffusion rate will be slowed down, and the oxidation will be affected by the nanocrystallinity, leading to either core/shell Co/CoO particles or hollow particles of CoO. (7) The effect of the nanocrystallinity on ordered nanoparticles exposed to oxidation has not been considered this extensively in previous research.

1.1. Purpose

The purpose of the thesis is to investigate the control of nanocrystallinity through analysis of the oxidation process of cobalt nanocrystals upon change in the crystalline structure of the nanoparticles and their assemblies, and also to examine how nanocrystal size affects the oxidation process.

Investigations of four different cobalt samples have been made, fcc and hcp synthesized by reverse micelle route, and fcc and ε formed by organometallic synthesis. The difference between the two fcc samples, synthesized by different the routes, is that the reverse micelle route results in the formation of smaller crystalline domains and thereby a more poorly crystallized structure, called small domain polycrystal, than the organometallic synthesis. The two fcc structures therefor differ in nanocrystallinity, as their domain size differs and the one with smaller domain size is closer to an amorphous structure, even if they are both fcc and polycrystalline.

1.2. Limitations

Oxidation, annealing and characterization are a part of the thesis work however synthesis of the Co-nanoparticles will not be included, but provided by the lab. For this reason, no synthetic routes will be presented as the focus has been on the characterization and of the nanoparticles. Metallic cobalt has three different crystal structures, which are all described more thoroughly in chapter 2.2, and the three possible structures have been tested.

Nanocrystallinity dependency will be investigated using nanoparticles with a size of 8 nm and how size affect the oxidation process will be examined for three different sizes, 4, 6 and 8 nm and only for two of the samples, the crystal structures fcc and hcp synthesized by the reverse micelle route. The reason why size dependency is not performed for all the samples is that there is not yet a successful method to obtain a good enough size control for the smaller particles made by the organometallic synthesis.

HRTEM has been performed on the samples before oxidation and for the samples oxidized at 200°C for 10 minutes but not for the samples oxidized at 260°C for the same time. The reason for this is that the HRTEM is a time consuming process and the instrument can only be run by trained people. In the end the time was not enough and the 200°C oxidation treatment was prioritized.

1.3. Outline of the thesis

The report is divided into five chapters, chapter 2, Theory, is presenting the necessary background information needed to understand the experimental methods and the oxidation behavior. It deals with the diffusion behavior described by the Kirkendall effect, the different structures of cobalt and cobalt oxides, the self-assembly and the colloidal stabilization necessary to prevent the particles from coalescence. Chapter 3 deals with the methods which in more elaborated terms mean the experimental procedure and the description of the methods for characterization, Transmission electron microscopy (TEM), High Resolution TEM (HRTEM) and electron diffraction (ED). Chapter 4, Results and Discussion, is divided into two parts. The first part handles the effect of nanocrystallinity and self-ordering while the second part presents the results regarding the size effect. The thesis is ended with chapter 5, conclusions, concluding the work and suggesting further areas of investigations.

2. Theory

The theory chapter contains background about the Kirkendall effect used to create hollow CoO or core/shell Co/CoO, information about the three different crystal structures of metallic cobalt and cobalt oxide, and the theory behind the self-assembly used to deposit samples on TEM grids for characterization.

2.1. The Kirkendall effect

During solid state reactions, diffusivity is a kinetically determining factor. Charge and size of the particles taking place in the reaction control the diffusivity. If two particles with different diffusivity react with each other the reaction will be faster in one direction than the other. This is known as the Kirkendall effect and results in a motion of the boundary layer that can be used to produce hollow nanoparticles. Oxygen is a large and charged ion and even though the metal ions in the lattice are also charged, the smaller size of the metal ion compared to the oxygen is what most often make up for the diffusion difference. This causes the metal ions to migrate outwards rather than the oxygen ions to migrate into the metal lattice, the created vacancies migrate inwards and can form a single interior cavity. (10)

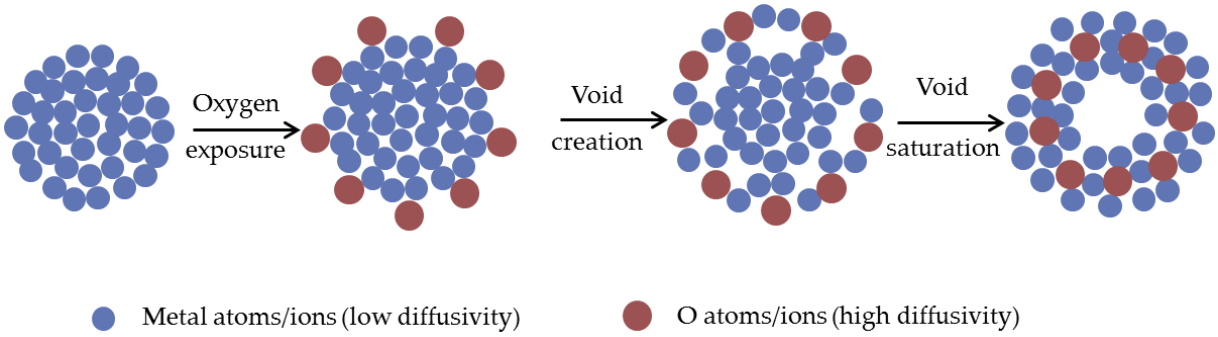

Figure 1. The nanoscale Kirkendall effect. The metal nanocrystal is reacted with oxygen and because of the faster outward diffusion of metal than the inward diffusion of oxygen voids are formed in the lattice. The voids are saturated in the center leading to a hollow nanocrystal.

The Kirkendall effect is known for causing weakness within a bulk material as it is the reason for internal void formation and thereby weakening of the material, but on the nanometer scale it can be used to create hollow nanoparticles instead, because of super saturation of vacancies into a hollow core (3), (11)., see Figure 1. The nanoscale Kirkendall effect is more complex than on a macroscale since the nanoscale system include factors like a shorter diffusion length, interface stress and inhomogeneous coating, all of which are less significant on a macroscale. Diffusion is made easier by defects in the lattice, like grain boundaries, since this enables atomic jumps. A hollow core formation can be prevented the produced phase being rich in defects which can absorb the vacancies without forming voids or by the particle being too small to be stable as a hollow structure. (11)

2.2. Crystal structures of metallic cobalt

Cobalt is a transition metal and that can be found between iron and nickel in the periodic system of elements and it is naturally occurring in the crust of the earth (2). Metallic cobalt has three possible crystal structures, the hexagonal closed-packed (hcp), face-centered cubic (fcc) and epsilon phase (ε) (12). The three phases are shown in in Figure 2 A-C. At normal pressure, two crystal structures are stable for bulk Co, the hcp below 425°C and the fcc at higher temperatures (2), (13). Because of a low free energy exchange, the change into the more stable hcp in room temperature is very slow (2).

Metastable phases such as ε-Co nanocrystals are possible to form in solution phase chemical synthesis because it is as a general rule not controlled by thermodynamics.

The hcp structure is constructed of layers in an ABABAB-stacking sequence, this leaves small channels in the structure between the Co-atoms. The fcc structure has an ABCABC-stacking sequence, making it cubic. The ε-phase is composed of two different geometrical arrangements, having the cubic structure of β-manganese, some distances are shorter than others and the purple and blue atoms in Figure 2 C have their neighboring atoms arranged differently.

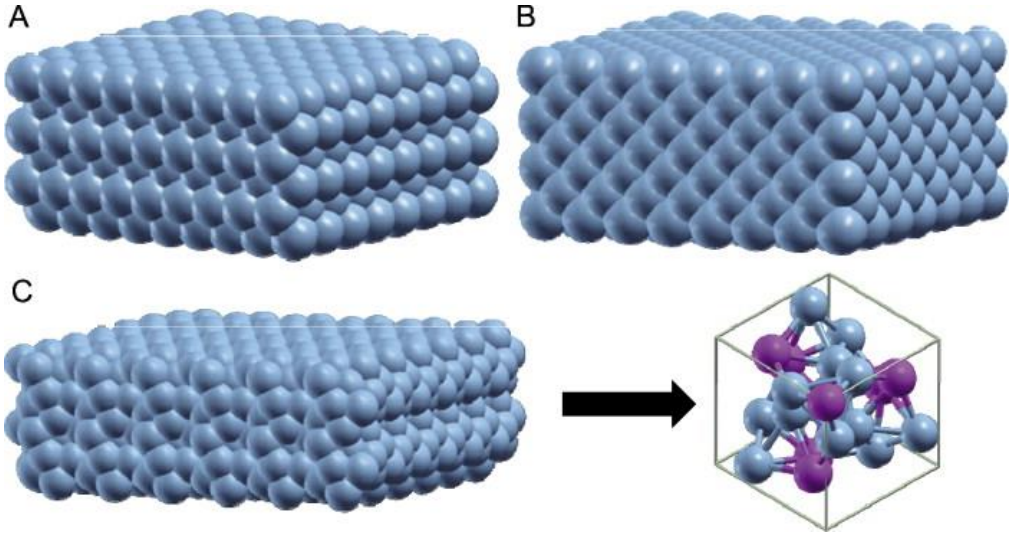

Figure 2. Sketch view of different bulk cobalt structures: (A) hcp or α, (B) fcc or β, (C) ε, (including a detail of the different cobalt position). [From reference (12), Reprinted with permission from American Institute of Physics. © *2010 American Institute of Physics*.]

During annealing, heat treatment, of a Co sample at a temperature below 425 °C the metal ions in the lattice becomes more mobile than in room temperature. This causes the ε or fcc lattice to transform into the more stable hcp structure (6), (14). The mechanics behind the change is due to dislocation movements of the octahedral planes of the cubic fcc or ε lattice (2).

Single domain crystals are built up by one single crystal, while polycrystals are built up by two or more fused crystals which mean that grain boundaries are present within a polycrystal. Magnetic properties of nanocrystals depend strongly on both particle size and the crystal structure. The complex cubic structure of the ε-Co nanocrystal is a soft magnetic material meaning the coercivity is low and the required force to demagnetize the material after it has been magnetized is low (6). The hcp is ferromagnetic at all temperatures, and the magnetic behavior remains after the source of the alignment of the electric dipoles has been removed. However the fcc becomes paramagnetic at 1121 ± 3°C, resulting in the consequence that the electric dipoles orient randomly after the removal of the magnetic field above the given temperature. Single crystalline hcp is magnetically anisotropic and will be more easily magnetized in on direction than the other, while the cubic structures have an isotropic magnetic behavior. The magnetic behavior of polycrystalline particles depend both of the purity of the metal and the thermal history of the material (2).

2.3. Structures of Cobalt oxides

Cobalt oxide complexes have been traditionally used as dying agents in the ceramic and glass production, it adapts different color depending on the metal ion binding together with the cobalt oxide. The density for the oxides is lower than for metallic cobalt leading to a growth in size of cobalt nanoparticles during oxidation (2).

Cobalt has two readily available oxidation states, Co^{2+} and Co^{3+}, and cobalt oxides exist in two main structures. The structurally most simple one is cobalt(II)oxide (CoO) which has a rock salt structure, meaning one Co^{2+} is octahedrally coordinated to the oxygen atoms in the lattice, with a = 0.425 nm. The structure is stable above 900 °C and is antiferromagnetic at normal temperatures. CoO has a density of 6.44 g/cm^3 at 20°C (15).The second main structure is cobalt(II,III)oxide (Co_3O_4), it is divalent and has a spinel structure with tetrahedrally coordinated Co^{2+} and octahedrally coordinated Co^{3+}, with a = 0.807 nm. It is the thermodynamically stable form of cobalt oxide under ambient temperature and pressure (1), (2), (16). The larger separation between the lattice fringes means that Co_3O_4 has a lower density than CoO with a value of 6.11g/cm^3 at 20°C (15).

Cobalt oxide exists in a third composition as well, the cobalt(III)structure (Co_2O_3), it is unstable but impure forms have been prepared. There is never a transition from Co_3O_4 into Co_2O_3, but the chemistry of Co(III) is instead dominated by formation of other chemical complexes (1), (2), (16).

The oxides can exist as either poly- or single crystalline structures which will affect their properties (2). Polycrystals can be used in catalysts or as nanoscale reactors as the grain boundaries enable a possible route for diffusivity of small particles (8).

2.4. Evaporation-induced self-assembly

The compact hexagonal 2D networks studied in the project are self-assembled through evaporation-induced self-assembly. A stable colloidal dispersion of Co nanocrystals is deposited on a surface and the solvent is allowed to evaporate. The ordering takes place in the meniscus, which is the curved surface formed at the top of the liquid, and because of the small volume of it, the nanocrystals are forced together. The two most important repulsive interactions of the system are the steric hindrance from the surfactants covering the surface of each nanocrystal due to reduced entropy and the osmotic flow of solvent towards the compressed region, and the columbic repulsions due to the same signs of the surface charges. The two forces together maximize the distance between the nanocrystals which creates an ordered compact network. (10)

2.4.1. Colloidal stabilization by oleic acid

All samples presented in the report are coated with oleic acid, $C_{18}H_{34}O_2$, see Figure 3. Steric stabilization is necessary to avoid aggregation in the colloidal dispersion and the carboxylic group in oleic acid binds strongly to the particle surface and forces the long hydrocarbon chain out into the non-polar solution (17). The long hydrocarbon chain probably also has an effect on the oxygen diffusion as is will work as a barrier for the nanocrystal and a protection against oxidation as well as aggregation. Oleic acid has a melting point at 13 – 14°C and a boiling point at 194 – 195°C (18).

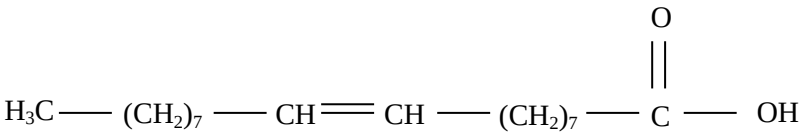

Figure 3. Chemical structure of oleic acid.

3. Method

The chapter describes the experimental procedure, the characterization methods and statistics. The experimental procedure starts with an overview before going into the different steps, after which characterization methods are presented one by one before a short section on how statistical certainty was achieved during analysis.

3.1. Experimental Procedure

Investigation of four different nanocrystalline cobalt samples have been performed, fcc synthesized by reverse micelles, which is a polycrystal with small crystalline domains (sample 1), hcp synthesized by reversed micelles, which has a single crystalline structure (sample 2), fcc formed by organometallic synthesis, which is a polycrystal (sample 3) and ε formed by organometallic synthesis which has a single crystalline structure (sample 4). The four investigated samples are summarized in Table 1 below. The difference between the two fcc samples, synthesized by the different routes, is that the reverse micelle route results in the formation of smaller crystalline domains and thereby a more poorly crystallized structure, called small domain polycrystal, than the organometallic synthesis. The two fcc structures therefor differ in nanocrystallinity, as their domain size differs and the one with smaller domain size is closer to an amorphous structure, even if they both have the fcc structure and are polycrystalline.

Table 1. Summary of investigated samples, their structure, nanocrystallinity and the synthetic route for formation.

Sample no.	Structure	Nanocrystallinity	Synthetic route	Size (nm)	Abbreviation
1	fcc	Small domain polycrystal	Reverse micelle	4, 6, 8	$Co_{poly\text{-}RM}$
2	hcp	Single domain	Reverse micelle	4, 6, 8	$Co_{HCP\text{-}RM}$
3	fcc	Polycrystal	Organometallic synthesis	8	$Co_{poly\text{-}ORG}$
4	ε	Single domain	Organometallic synthesis	8	$Co_{\varepsilon\text{-}ORG}$

The stabilizer of the colloidal dispersion was in all four cases oleic acid, which is described in chapter 2.4.1. Comparison of the nanocrystallinity effect was performed with nanoparticles in the size of 8 nm and the size effect has been examined using three different sizes, 4, 6 and 8 nm, of fcc and hcp synthesized by the reverse micelle route. Characterization of the nanoparticles was executed using TEM, HRTEM and electron diffraction.

Sample 1, 3 and 4 were synthesized in a glove box with nitrogen atmosphere to avoid oxidation of the nanoparticles. To achieve the hcp structure of sample 2, sample 1 was dry-phase annealed in 250 °C under argon flow for 60 minutes. All samples were oxidized in 200˚C or 260˚C for ten minutes and characterized with TEM and ED both before and after oxidations to investigate how the oxidation procedure had been affected by the nanocrystallinity, the self-ordering and the nanocrystal size. HRTEM was performed on all samples after oxidation to receive more information about the oxidation behavior. A summary of the experimental procedure is presented in the flowchart in Figure 4.

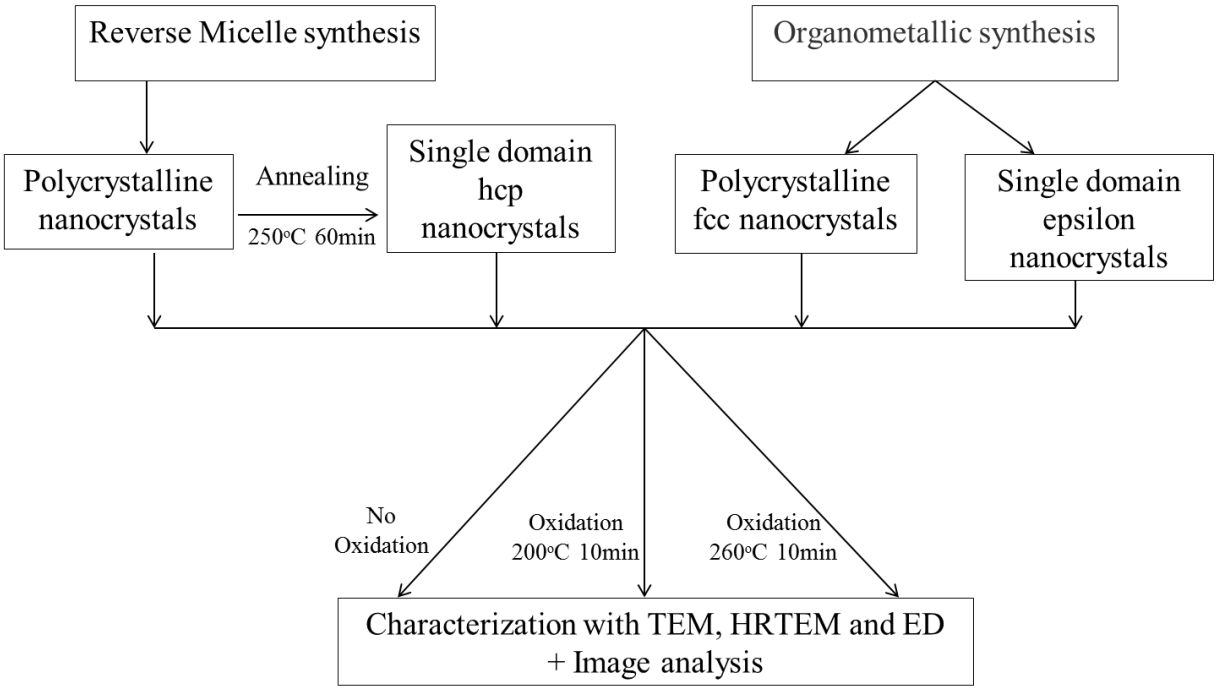

Figure 4. Flow chart of experimental procedure for investigation of how nanocrystallinity, self-ordering and nanocrystal size affects the oxidation of Co nanocrystals.

3.1.1. Sample preparation for TEM

The sample was prepared in a glove box with inert nitrogen atmosphere. The sample, containing Co-nanoparticles coated with oleic acid in hexane, was deposited on the TEM grid (copper grid coated with amorphous carbon film) and left for two minutes allowing the solvent to evaporate causing the Co-nanoparticles to self-assemble into a monolayer. The grid was placed in the sample loader and inserted into the TEM for characterization.

3.1.2. Dry phase annealing

The samples were annealed through dry phase annealing, meaning that the particles were already deposited and ordered into a 2D lattice on the TEM grid when exposed to the heat treatment. The grid with the applied sample was placed in a tube and loaded on a modified Schlenk line, which included a high vacuum pump, a source of inert argon gas and a source of oxygen gas. The sample was exposed to vacuum then Ar flow in three rounds to ensure that all air had been removed from the system. The heater was adjusted to 250 °C and the annealing took place under argon flux for 60 minutes, after which the heater was removed to stop the annealing. The sample was left to cool to room temperature by the argon flow (10 min).

3.1.3. Dry phase oxidation

The grid with sample on it was placed in a tube and loaded on the modified Schlenk line, the same used during annealing, and treated with O_2 (200˚C, 10 min or 260˚C, 10 min). After oxygen treatment the heater was removed, the oxygen flow was replaced by argon flow to stop the oxidation immediately and the sample was allowed to cool to room temperature by the argon flow (10 min).

3.2. Characterization

Methods used for characterization of the Co-nanoparticles, both before and after the two oxidations, are TEM, HRTEM and ED. The methods are described in the two following subchapters.

3.2.1. Transmission Electron Microscopy (TEM)

The analysis is performed in a vacuum chamber. A high energy beam of electrons is directed towards a thin sample of the particles assembled on a copper grid coated with an amorphous carbon film. The electrons that are transferred through the sample are detected and form a two dimensional projection of the sample. The instrument can be chosen to detect either the direct beam (bright field image) or the diffracted beam (dark field image) (19). TEM can be used as a high resolution instrument to detect the size and shape of the particles, but not to determine the 3D structure of the lattice.

TEM is available in different modes, depending on what instrument is used. In High Resolution mode (HRTEM), the electrons are accelerated with a higher potential field, giving them a shorter wavelength and higher energy which increase the resolution of the obtained image (19). This way the lattice planes of a nanocrystal oriented in the right direction can be seen.

TEM was performed using a JEOL 1011 microscope at 100 kV, and HRTEM was performed using a JEOL 2010 microscope at 200 kV.

3.2.2. Electron diffraction (ED)

Electron diffraction (ED) is available in the TEM instrument and can be used to determine the crystal structures of the nanocrystals. Electrons are fired at the sample and the resulting interference pattern is observed as the incoming primary electrons interact with the secondary electrons reflected off the lattice planes. Electron diffraction can be used to calculate the interplanar distance between lattice planes and can thereby be used to determine the crystal structure (20). The diameter of the resulting rings in the ED patterns are measures and the inverse value of the radius can be compared to theoretical values to determine, confirm or deny the crystal structure.

3.3. Statistics

To measure size of the full diameter or the internal structure and achieve histograms and size distributions of the nanocrystals both before and after oxidation, at least 500 nanocrystals were measured on the TEM images for each sample, using the free software ImageJ. The histograms were prepared using Origin8. In the cases where the percentage of hollow, core/shell or fully oxidized particles are presented, at least 500 nanocrystals were investigated, using the TEM images.

4. Results and Discussion

The chapter is divided into two main subchapters, the first one, chapter 4.1, concerns the investigation on how the nanocrystallinity affects the oxidation behavior and the second one, chapter 4.2, is about how the size of the nanoparticle affects the oxidation behavior. Both subchapters deal with the question on how the self-ordering affects the end results. The nanocrystallinity dependency is examined using 8 nm particles for all four different samples while the size effect is evaluated using 4, 6 and 8 nm particles of $Co_{poly\text{-}RM}$ and $Co_{HCP\text{-}RM}$. The expected result before the start of the investigation was to find a change within the oxidation of the various single domains and between the single- and polycrystals.

4.1. Nanocrystallinity dependency

The results regarding the 8 nm particles for each of the four different nanocrystallinities are presented separately for each sample and discussed in the text. The samples are all presented before oxidation, after oxidation at 200°C for 10 minutes and after oxidation at 260°C for 10 minutes. After the last sample a more general discussion is made, taking all the results into account and trying to answer how nanocrystallinity and self-ordering affects the oxidation behavior of cobalt nanocrystals.

4.1.1. Polycrystalline nanocrystals produced from reversed micelles ($Co_{poly\text{-}RM}$)

The polycrystalline nanocrystals synthetized by the reverse micelle route ($Co_{poly\text{-}RM}$) are characterized by very small fcc domains that indicate a very low crystallinity. No evidence can be given to prove that some domains are not amorphous. In Figure 5a, a $Co_{poly\text{-}RM}$ nanoparticle is visualized in a HRTEM image. No crystalline domains are clearly seen as they are too small to appear as an ordered structure in the images, this indicates that the crystallinity is not well defined.

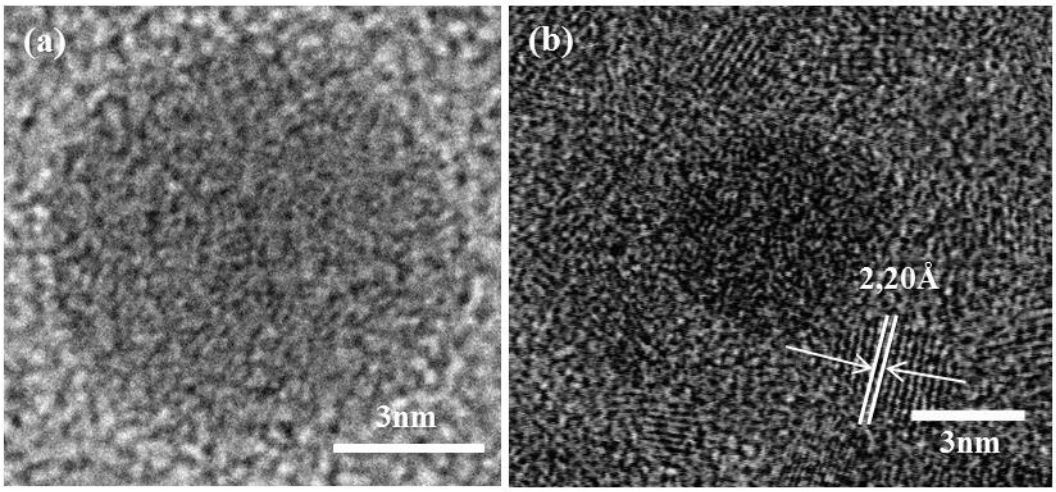

Figure 5. HRTEM images from polycrystalline nanocrystals produced from reversed micelles ($Co_{poly\text{-}RM}$) 8 nm. (a) Native nanoparticle before oxidation, no lattice planes can be perceived which indicates low crystallinity, (b) After oxidation at 200°C for 10 min. Core/shell $Co_{poly\text{-}RM}$/CoO nanoparticle showing the lattice plane (200) for CoO in the shell.

Figure 6a and 6b show the TEM images at various scales of the nanocrystals in their native state before oxidation. The observed zone is well ordered in a compact hexagonal network with some isolated nanocrystals, giving the opportunity to study how the 2D ordering affects the oxidation. From the histogram (inset Figure 6a) the nanocrystal size and its distribution are 8.3 ± 0.77 nm and 9.3% respectively. The electron diffraction (ED) pattern (Figure 6c) shows only one clear ring corresponding to the fcc lattice plane (111). This confirms the information from the HRTEM image of the same sample in Figure 5a in which the crystallinity of the nanoparticles is not well defined.

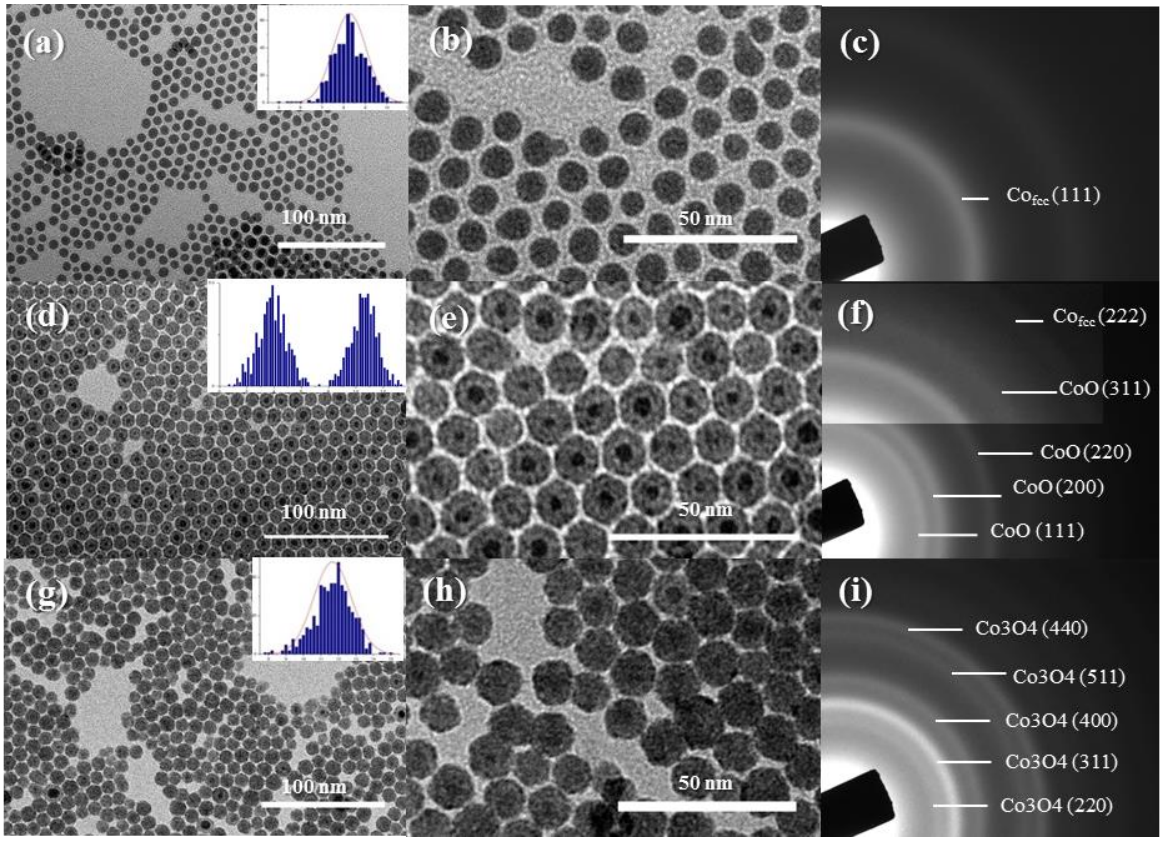

Figure 6. Polycrystalline nanocrystals produced from reversed micelles ($Co_{poly\text{-}RM}$), 8 nm. (a, b) TEM images before oxidation, (d, e) after oxidation at 200˚C for 10 min, (g, h) after oxidation at 260˚C for 10 min. (c, f, i) Corresponding ED pattern before and after the two oxidation temperatures. The insets in (a, g) are histograms displaying the size distributions of the nanoparticle diameter, in (d) the histogram displays both the particle diameter and the diameter of the core in the core/shell nanoparticle.

The TEM images of the sample submitted to oxidation at 200°C for 10 minutes reveals formation of both core/shell ($Co_{poly\text{-}RM}$/CoO) and CoO nanocrystals (Figure 6d and 6e). The average diameter of nanocrystals is 10.6 ± 0.98 nm, with a size distribution of 9.2%, which is almost equal to the distribution observed before oxidation (9.3%) even if the nanoparticles have grown. The average diameter of the core proved to be 3.9 ± 1.07 nm, with a size distribution of 27.8%. The calculated thickness of the oxide shell is thereby 3.4 nm, however, there is large size distribution of the core making the calculations uncertain. From HRTEM image (Figure 5b) it can be seen that the crystalline structure of Co core remains similar as that observed before oxidation while the oxidized shell shows a polycrystalline structure with a lattice plane corresponding to the CoO (200). A particle in more highly ordered areas of the lattice has the tendency to become core/shell during oxidation, but along the edges of the monolayer and in the regions where the nanocrystals are not well ordered, most of the nanocrystals are fully oxidized.

In Figure 7a, a small assembly of nanoparticles is visualized, it is clearly seen that the nanoparticles in the middle of the assembly are core/shell while the edges of the assembly consists of nanoparticles with a smaller core or are fully oxidized. It can be noticed that isolated nanoparticles are mostly fully oxidized, but some size dependency can be seen among them, where larger particles received a core/shell structure while smaller particles were fully oxidized. In Figure 7b two isolated particles show a core/shell structure with a very small core. A general feature is that the larger the nanoparticle size is, the larger the core becomes in the core/shell structure for both ordered and isolated structures. The size effect of the $Co_{poly\text{-}RM}$ has been further investigated in chapter 4.2.1. The ED pattern (Figure 6f) displays rings for both CoO and fcc-Co supporting the information given by the HRTEM image

that a core shell structure with both the fcc-Co and CoO is present. However, only the outer rings of the fcc lattice can be seen but as fcc (111) and (220) is close in d-spacing to CoO (200) and (311) they can be hidden behind each other, or the rings for the fcc lattice can also be unclear because of the nearly amorphous structure. The separation between the lattice planes is larger for CoO than fcc-Co, and this change in density explains the growth during oxidation (2), (15).

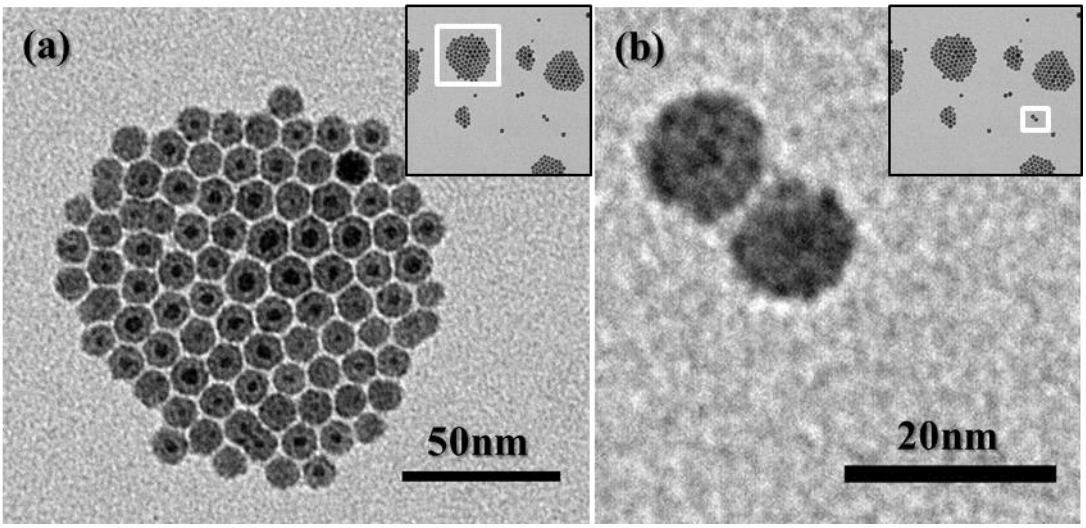

Figure 7. Polycrystalline nanocrystals produced from reversed micelles ($Co_{poly\text{-}RM}$), 8 nm, after oxidation at 200˚C for 10 min. (a) TEM images of small assembly of nanoparticles. (b) TEM image of isolated particles. The inset is the corresponding low magnification TEM where the enlarged image is selected from the white rectangle.

When the oxidation process takes place at 260°C instead of 200°C, keeping the same exposure time (10 min) some core/shell structure is still present, but most of the nanoparticles have become fully oxidized (Figure 6g and 6h). The size of the particles has increased to 11.7 ± 1.09 nm but keeping the distribution of 9.3%. According to the corresponding ED pattern (Figure 6i) the oxide has obtained the spinal structure, Co_3O_4, in contradiction with the oxidation at 200°C where the nanoparticles received the cubic CoO structure. The space between the nanoparticles decreases on increasing the temperature and consequently the tendency of nanocrystals to coalescence increases. This can be due to the faster oxidation at 260˚C compared to 200˚C or a consequence of the smaller space between the lattice planes and thereby lower density of the Co_3O_4 compared to the CoO (15).

In conclusion, $Co_{poly\text{-}RM}$ nanocrystals produced from the reverse micelle route is highly polycrystalline and thereby presents many grain boundaries for possible oxygen diffusion. As the oxygen diffusion becomes fast, the inward diffusion can compete with the outward diffusion of Co atoms and no internal void is formed. The oxidation thereby results in a core/shell particle. In the case that internal pores are formed they can be annihilated in the high concentration of grain boundaries without forming an internal void (11). In the less ordered areas the $Co_{poly\text{-}RM}$ nanoparticles are exposed to more oxygen compared to the nanoparticles in the more highly ordered areas, as the nanoparticles are not being protected from the oxygen by the neighboring particles on the sides, resulting in fully oxidized nanoparticles instead of the core/shell particle. These data are in agreement compared to those already obtained with 7nm $Co_{poly\text{-}RM}$ nanoparticles performed earlier by the same group (7). The higher oxidation temperature of 260˚C speeds up the oxidation, which results in a higher concentration of fully oxidized particles compared to after the lower oxidation temperature 200˚C.

4.1.2. Single domain hcp nanocrystals produced by annealing Co nanoparticles from reverse micelle approach ($Co_{HCP\text{-}RM}$)

Single domain crystalline hcp ($Co_{HCP\text{-}RM}$) are produced by annealing $Co_{poly\text{-}RM}$ nanoparticles. Figure 8a and 8b show TEM images with well-defined nanocrystals with an average size and distribution of 8.4 ± 0.85 nm and 10.1% respectively. The size is slightly larger than what was observed for $Co_{poly\text{-}RM}$

nanoparticles (8.3 ± 0.77 nm and 9.3%), but the small change is within the margin of error of the measurements. Figure 9a shows the HRTEM images for Co_{HCP-RM} before oxidation, the ordered lattice planes correspond to the hcp-Co (002) and the nanocrystal is built up by one single crystalline domain. No sign of oxidation from the annealing treatment can be seen as this would have shown on the HRTEM image and also have generated a ring, characteristic for CoO, inside the inner triplet rings in the ED pattern (Figure 8c).

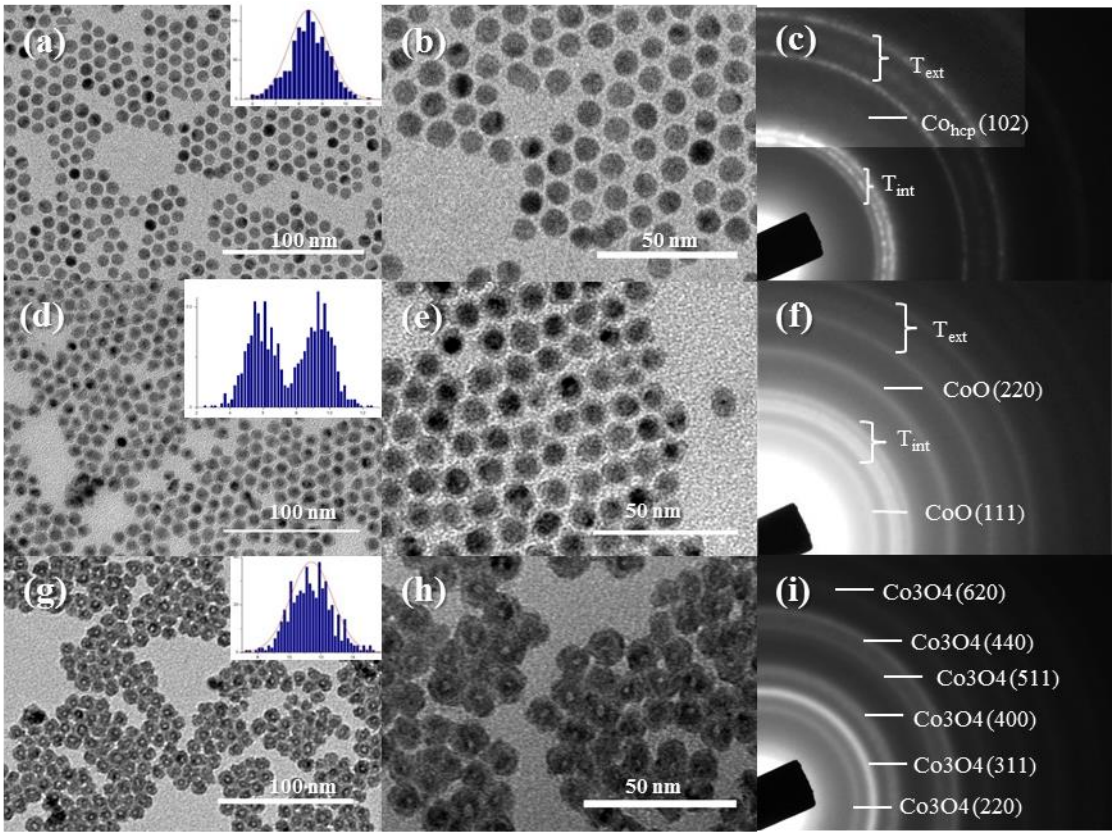

Figure 8. Single domain hcp nanocrystals produced by annealing Co nanoparticles from reverse micelle approach (Co_{HCP-RM}) 8 nm. (a, b) TEM images before oxidation, (d, e) after oxidation at 200°C for 10 min, (g, h) after oxidation at 260°C for 10 min. (c, f, i) Corresponding ED pattern before and after the two oxidation temperatures. T_{int} and T_{ext} marked on the ED pattern in (c) and (f) refer respectively to the internal triplet rings [(100), (101), (002)] and external triplet rings [(110), (103), (112)], of the hcp lattice. The insets in (a, g) are histograms displaying the size distributions of the nanoparticle diameter, in (d) the histogram inset displays both the particle diameter and the diameter of the core in the core/shell nanoparticle.

The Co_{HCP-RM} nanocrystals are submitted to same treatment as the previously described nanoparticles (oxidation at 200°C; 10mn). For any ordered nanocrystal a core/shell Co_{HCP-RM}/CoO structure is observed (Figure 8d and 8e), but for isolated nanocrystals either core/shell or fully oxidized nanocrystals are produced. The thickness of the shell is thinner when the nanocrystals are ordered compared to when they are isolated, this behavior is visualized in Figure 8e with the single isolated particle having a smaller core, and thereby a thicker shell, than the neighboring ordered particles. Furthermore, the shell is thinner for the largest nanocrystals compared to smaller one when both are ordered in compact hexagonal network. The nanocrystals have a mean diameter of 9.4 ± 0.88 nm and a size distribution of 9.4%, the average diameter of the core for ordered nanoparticles is 5.8 ± 0.91 and has a distribution of 15.7% this gives the average shell thickness of 1.8nm. The HRTEM image (Figure 9b) shows that the large core keeps its former crystalline structure. It has a regular pattern of lattice planes that correspond to the hcp-Co (002) plane. The oxide shell shows two different distances for the CoO lattice, 2.13 Å corresponding to the (200) plane and 2.46 Å corresponding to the (111). The corresponding ED pattern (Figure 8f) illustrates a mixture of both hcp-Co and CoO which supports the information from the TEM and HRTEM pictures of a core/shell Co_{HCP-RM}/CoO structure. These data are reproducible and surprising if compared to a previous study performed by the same group with 7 nm Co_{HCP-RM} nanoparticles instead of 8 nm. For the 7 nm nanoparticles, hollow CoO

single domain nanocrystals were produced (7). The effect of size on the oxidation behavior of Co_{HCP-RM} has been investigated further in chapter 4.2.2.

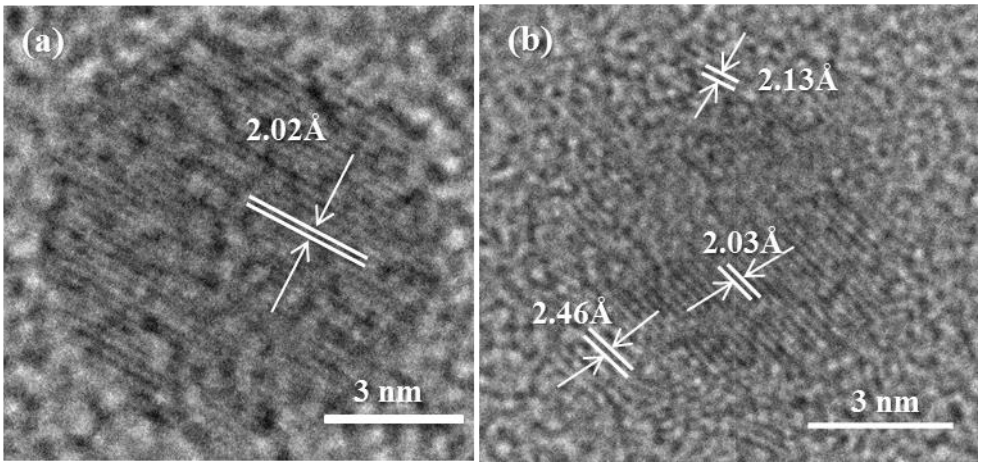

Figure 9. HRTEM images from single domain hcp nanocrystals produced by annealing Co nanoparticles from reverse micelle approach (Co_{HCP-RM}) 8nm. (a) Before oxidation, single domain nanoparticle showing the lattice planes for the hcp (002) plane. (b) After oxidation at 200˚C for 10 min. Core/shell Co/CoO nanoparticle showing the lattice planes for the hcp core (002) and the CoO shell (111) and (200).

When the temperature is increased to 260°C instead of 200°C, keeping the same exposure time, the nanoparticles tend to coalesce (Figure 8g and 8h). However, it is shown that the nanoparticles present hollow structure with a thick oxide shell and an internal void. An increase in the size can be seen after oxidation at 260˚C compared to after 200˚C as the particles are now 11.4 ± 1.33 nm with a distribution of 11.7%. The ED pattern (Figure 8i) shows formation of the spinal structure Co_3O_4 instead of CoO. The difference in sizes observed between the sample oxidized in 200°C and in 260°C is explained by the fact that Co_3O_4 has lower density compared to CoO and also that a more rapid oxidation and consequently a faster oxygen diffusion takes place after increasing the temperature. The creation of an internal void is also a factor that leads to a larger increase in the outer diameter

During the annealing process it is likely that some of the oleic acid used as a coating agent is broken down, but as no fusion of the Co can be seen after the annealing, some coating must still be intact surrounding the nanoparticles and making them avoid aggregation. The partly broken oleic acid can be the reason that Co_{HCP-RM} oxidized at 260°C for 10 min coalescence more than $Co_{poly-RM}$ after the same oxidation treatment. However, the formation of an internal void for Co_{HCP-RM} and thereby a larger increase in the size is also a reason for enhanced coalescence. It can clearly be seen that 200°C for 10 minutes does not produce a fast enough outward movement of cobalt compared to the inward movement of oxygen to create hollow nanoparticle for the 8 nm structure.

If Co_{HCP-RM} is compared to $Co_{poly-RM}$ (chapter 4.1) for the 8 nm nanoparticles, they differ in their oxidation behavior. Both samples form core/shell structures after oxidation at 200°C for 10 min but the size of the cores are larger for the hcp single crystalline structure than the polycrystalline nanoparticle, and the size change during oxidation is smaller for the single domain nanocrystal. The difference can clearly be seen when comparing the thickness of the oxide shell. For $Co_{poly-RM}$ the shell thickness is 3.9 nm while Co_{HCP-RM} displays a thickness of 1.8 nm. The difference can be an indication that oxygen atoms have a slower diffusion path in to the hcp single crystal lattice than the polycrystalline lattice. Because of the low crystallinity many grain boundaries are present in the polycrystalline lattice while no grain boundaries are present in the single crystalline hcp lattice. The grain boundaries work as a fast diffusion path making the oxidation of easier for $Co_{poly-RM}$ than for Co_{HCP-RM}. A faster oxidation means a smaller core for the structure after oxidation and thereby a thicker oxide shell.

4.1.3. Polycrystalline fcc nanocrystals produced from organometallic synthesis ($Co_{poly\text{-}ORG}$)

The organometallic method is used to synthesize polycrystalline fcc-Co ($Co_{poly\text{-}ORG}$) with larger crystalline domains compared to those produced within the $Co_{poly\text{-}RM}$ nanocrystals, grain boundaries are thereby present, but not in as high concentration as for the sample prepared by reversed micelles. HRTEM images (Figure 10a) shows some grain boundaries, verifying the poly crystallinity of the sample, but if compared to $Co_{poly\text{-}RM}$ in Figure 5a, $Co_{poly\text{-}ORG}$ clearly has larger crystalline domains. The $Co_{poly\text{-}ORG}$ nanocrystals deposited on TEM grid shows mainly 2D super lattices and the formation of multilayers (Figure 11a and 11b) and very few isolated nanocrystals are detected. From histogram shown in the inset in Figure 7a, the average diameter of $Co_{poly\text{-}ORG}$ nanocrystals before oxidation is 8.1 ± 0.67 nm with a 7.1% size distribution. The ED pattern (Figure 11c) clearly shows presence of an fcc structure.

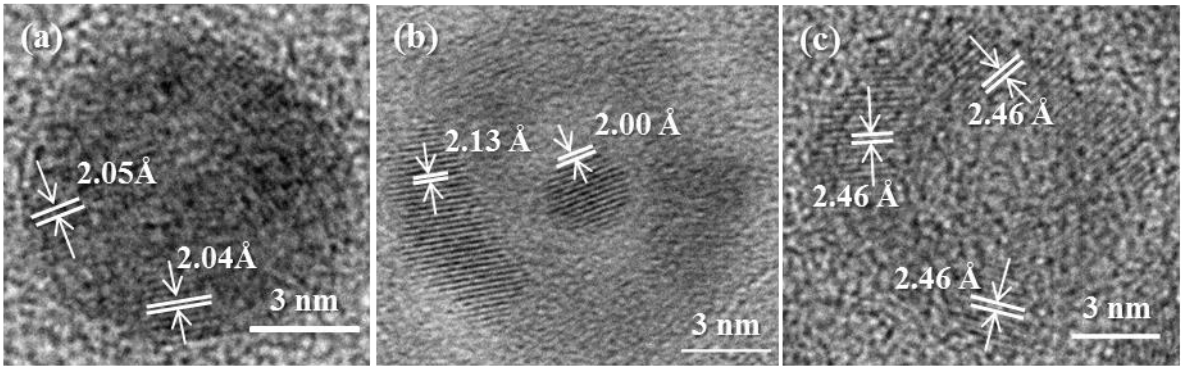

Figure 10. HRTEM images from polycrystalline fcc nanocrystals produced from organometallic synthesis ($Co_{poly\text{-}ORG}$) 8nm. (a) Before oxidation, lattice planes nanoparticle showing lattice planes for fcc-Co. (b) One of the obtained structures after oxidation at 200°C for 10 min, Core/shell Co/CoO particle showing the lattice planes for the fcc-Co core and the CoO shell, (c) the other obtained structure after oxidation at 200°C for 10 min, hollow particle showing the lattice planes of the CoO shell.

After submitting $Co_{poly\text{-}ORG}$ nanocrystals deposited on a TEM grid to oxidation (200°C; 10 min) both yolk/shell (Co-fcc/CoO), and hollow CoO nanoparticles were produced (Figure 11d and 10e). With the term yolk/shell means that the core is isolated from the shell and that the void is saturated between the core and the shell unlike a core/shell particle where the metal core and the oxide shell are in contact with each other. The average size of nanocrystals markedly increased compared to $Co_{poly\text{-}ORG}$ nanocrystals before oxidation. It is found equal to 10.7 ± 0.80 nm with a size distribution of 7.5% (inset Figure 11d). The HRTEM image shows a yolk/shell nanocrystal (Figure 10b) with the Co core isolated from the CoO shell by voids. The core shows a single domain crystalline structure with regular lattice planes corresponding to the fcc-Co (111) plane. The shell shows planes with a distance of 2.13 Å corresponding to the CoO (200) plane. It is not possible to know if CoO shell is single domain or polycrystals because the orientation of the shell could be such that only one side of the shell shows the lattice planes, and none of the two possibilities could be confirmed or ruled out by a careful HRTEM study. Figure 10c shows the formation of a hollow nanocrystal, after the same oxidation treatment, with a shell characterized by lattice planes with a distance of 2.46 Å corresponding to the CoO (111) plane. The oxide shell of the hollow particle is polycrystalline, as the directions of the (111) planes differ in different areas. From TEM images, under investigation of 500 nanoparticles in monolayers 62 % of nanocrystals are characterized by a yolk/shell structure and 38 % by hollow nanoparticles. The shape of the particles is more irregular after oxidation than before. The corresponding ED pattern (Figure 11f) supports the fact that both CoO and fcc-Co are present after oxidation.

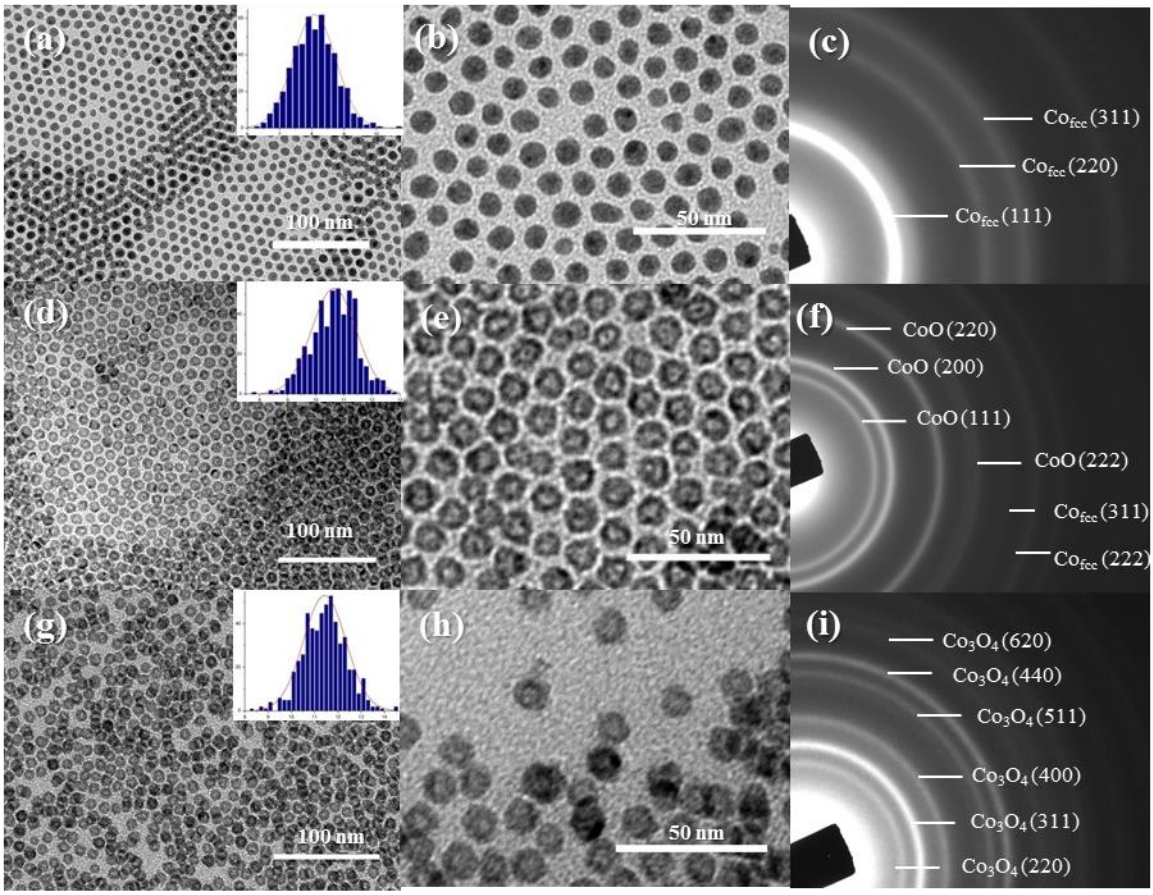

Figure 11. Polycrystalline fcc nanocrystals produced from organometallic synthesis ($Co_{poly\text{-}ORG}$) 8 nm. (a, b) TEM images before oxidation, (d, e) after oxidation at 200˚C for 10 min, (g, h) after oxidation at 260˚C for 10 min. (c, f, i) Corresponding ED pattern before and after the two oxidation temperatures. The insets in (a, d, g) are histograms displaying the size distribution at the different times.

The data after oxidation at 200°C for 10 min are rather surprising if compared to those obtained with same size of Co nanocrystals produced from reverse micelles ($Co_{poly\text{-}RM}$) with those produced from inorganic method ($Co_{poly\text{-}ORG}$). In both cases fcc domains are present before oxidation, however the $Co_{poly\text{-}RM}$ nanocrystals (Figure 5a) are characterized by small well-defined domains whereas with $Co_{poly\text{-}ORG}$ nanocrystals the fcc domains are larger (Figure 10a). Furthermore, it is observed that the size of crystalline fcc domains in the $Co_{poly\text{-}ORG}$ nanocrystals before oxidation changes from one nanocrystal to another. Such change within a given synthesis mode could explain the change in morphology obtained after oxidation and explain the formation of the two different structures, the yolk/shell and the hollow nanocrystals. With this in mind, the different structures obtained for $Co_{poly\text{-}RM}$ and $Co_{poly\text{-}ORG}$ nanocrystals respectively after oxidation at 200°C for 10 min could also be understood.

From a previous study performed by the same group (7) with 7nm $Co_{poly\text{-}RM}$ and $Co_{HCP\text{-}RM}$ nanocrystals we known that the relative diffusion of oxygen and Co in the nanocrystals markedly changes between hcp single domain and polycrystalline fcc phase. Here it becomes obvious that even though the structure remains similar (fcc), the size of the domains significantly change the diffusion process. We could assume, in first approximation, that with small fcc single domain the oxygen diffuse into the Co lattice keeping the integrity of Co core instead of the Co diffusing outwards and creating voids within the nanoparticle after oxidation treatment.

After oxidation at 260 °C for 10 minutes (Figure 11g and 11h) the majority of nanoparticles show a hollow structure, with some elements of yolk/shell particle with a small core. The assembly on the TEM grid was uneven and no conclusions about self-assembly could be made. The average nanocrystal (11.4 ± 0.92 nm with a distribution of 8.1%) increases compare that what observed under

oxidation at 200°C to the size after oxidation at 260°C, as expected. The void has a slight square shape compared to the circular nanoparticles before oxidation and this behavior can also be seen when viewing the particles after oxidation at 200°C. The corresponding ED pattern (Figure 11i) shows the presence of Co_3O_4 which means the elevated temperature causes the structure to transform to a spinel structure instead of the rock salt structure of CoO formed after oxidation at 200°C.

4.1.4. Single domain ε phase Co nanocrystals produced from organometallic synthesis ($Co_{\varepsilon\text{-ORG}}$)

Figure 12a and 12b show single domain ε phase Co nanocrystals ($Co_{\varepsilon\text{-ORG}}$) produced from organometallic synthesis deposited on a TEM grid with an average size of 8.1 ± 0.58 nm and with a size distribution of 7.1% (inset Figure 12a). The large and lighter monolayers are seen with some small areas being double or triple layers. From the HRTEM image in Figure 13a, it is clear that the nanoparticle consists of one single crystalline domain displaying the ε-Co (221) lattice plane. The corresponding ED pattern presents a triplet, characteristic for the ε-Co (221), (310) and (311) lattice planes.

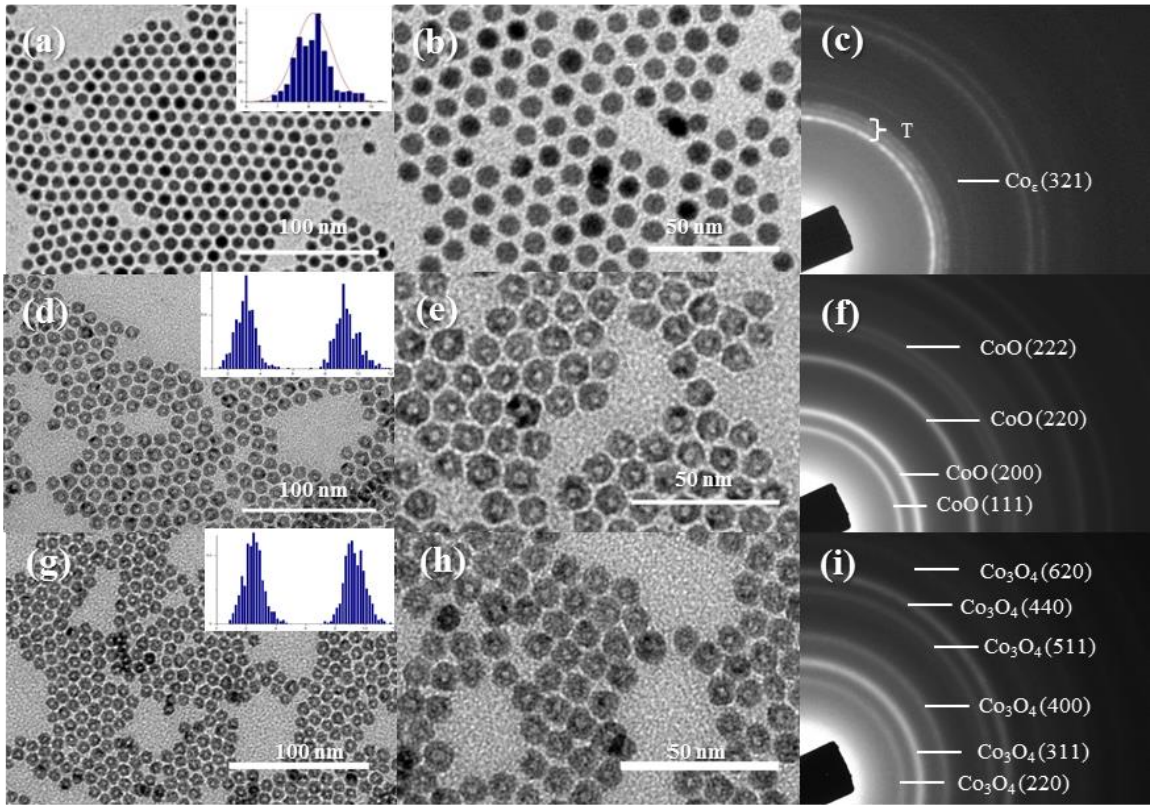

Figure 12. Single domain ε phase Co nanocrystals ($Co_{\varepsilon\text{-ORG}}$) produced from organometallic synthesis, 8 nm. (a, b) TEM images before oxidation, (d, e) after oxidation at 200˚C for 10 min, (g, h) after oxidation at 260˚C for 10 min. (c, f, i) Corresponding ED pattern before and after the two oxidation temperatures. T marked on the ED pattern in (c) refers to the triplet rings [(221), (310), and (311)] of the ε lattice. The inset in (a) is a histograms displaying the particle diameter and the histogram insets in (d, g) displays the particle diameter and the diameter of the void.

Like the others Co nanocrystals, the sample was submitted to an exposure of oxygen in the same experimental conditions as described above (200˚C; 10 min). The TEM images obtained after the oxidation process shows formation of hollow nanocrystals (Figure 12d and 12e). The mean diameter of the ε-Co nanoparticles increases compared to that obtained before oxidation and is found equal to 9.3 ± 0.75 nm with an 8.0% distribution. The increase in size is probably due to the outwards migration of Co-particles during oxidation which is what also creates the central void, with an average diameter of 3.1 ± 0.62 nm and a distribution of 20.2%. The two measurements reveal that the shell thickness is 3.1 nm. The hollow CoO exist in a large quantity and only a few single core/shell

structures are obtained within the nanocrystal monolayer and. Some areas show particles with larger voids within the more ordered areas of the lattice compared to particles in the less ordered areas. Because of the lower order, the sample is in contact with a higher concentration of oxygen which makes the inward diffusion of oxygen faster and therefor the internal void, caused by outward diffusion of Co atoms, smaller. The HRTEM image (Figure 13b) shows that the shape of the $Co_{\varepsilon\text{-ORG}}$ nanoparticles has become more irregular after oxidation at 200°C for 10 min compared to before oxidation (Figure 13a). The oxide shell shows regular lattice planes with a distance of 2.46 Å that correspond to the CoO (111) planes with two different directions. This means that the CoO shell is polycrystalline with two different crystalline domains. The corresponding image from the ED pattern (Figure 12f) shows a clear pattern from CoO, which proves the results visualized on the TEM and HRTEM images that a hollow CoO particle is created after oxidation at 200°C for 10 minutes.

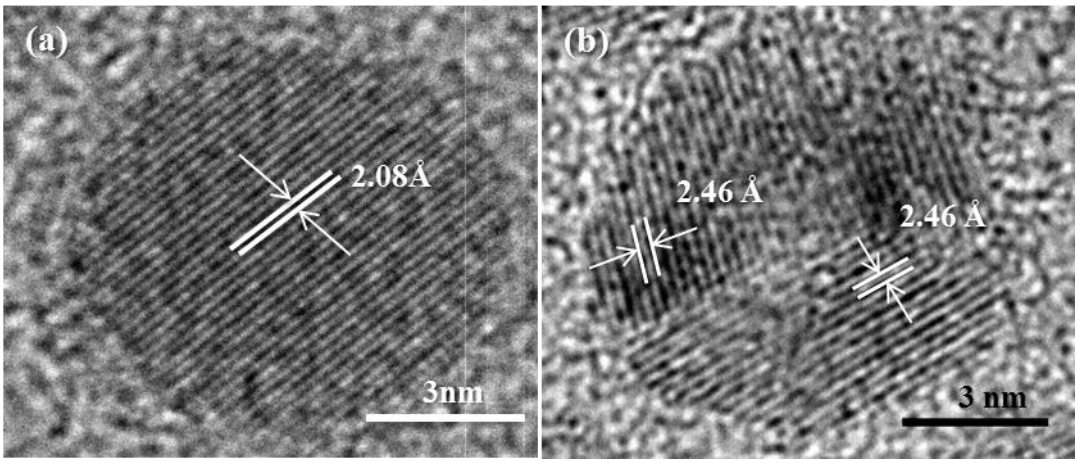

Figure 13. HRTEM images from single domain ε phase Co nanocrystals ($Co_{\varepsilon\text{-ORG}}$) produced from organometallic synthesis 8nm. (a) Before oxidation, single crystalline nanocrystal displaying the lattice plane from ε-Co. (b) After oxidation at 200˚C for 10 min. Hollow particle showing the lattice planes for the CoO shell.

On increasing the temperature to 260°C (with 10 min exposure), hollow particles are obtained in the TEM grid, like after the oxidation at 200°C and this can be seen in Figure 12g and 12h. The size of the nanoparticle is 9.3 ± 0.69 nm, with a 7.4% distribution (inset Figure 12g), while the void has a diameter of 2.5 ± 0.66 nm, with a distribution of 26.7%.This information was used to calculate the shell thickness to 3.4 nm. This is slightly larger than the oxide thickness after oxidation at the lower temperature (3.1 nm). The corresponding ED pattern (Figure 12i) reveals a change in the structure after the change in oxidation temperature as the oxide shell is now built up by the spinal structured Co_3O_4 instead of the cubic CoO. The distance between the lattice planes is larger for the spinal structures and this explains the thicker shell after oxidation at the higher temperature.

The ε phase of Co is not as stable as the two other structures. It is more easily oxidized by the electron beam in the TEM and it is likely that is also oxidizes easier during the oxidation treatment. The formation of the hollow structure leaves no trace of a core as the 8 nm samples for both $Co_{HCP\text{-}RM}$ and $Co_{poly\text{-}ORG}$.

4.2. Size dependency

The results from the three sizes 4, 6 and 8 nm are presented for polycrystalline nanocrystals produced from reverse micelle approach ($Co_{poly\text{-}RM}$) and single domain hcp nanocrystals produced by annealing Co nanoparticles from reverse micelle approach ($Co_{HCP\text{-}RM}$). Both samples, in the three sizes, are presented after the two oxidation treatments 200°C for 10 minutes and 260°C for 10 minutes.

4.2.1. Polycrystalline nanocrystals produced from reverse micelles ($Co_{poly\text{-}RM}$)

A comparison between the three different sizes, 4, 6 and 8 nm, of $Co_{poly\text{-}RM}$ nanocrystals after oxidation at 200°C is presented in Figure 14. The 4 nm particles have become fully oxidized CoO (Figure 14a), the 6 nm particles have formed both fully oxidized CoO particles and core/shell $Co_{poly\text{-}RM}$/CoO with a small core (Figure 14b), while the 8 nm particles almost only display a core/shell $Co_{poly\text{-}RM}$/CoO structure (Figure 14c). The larger the particle is before oxidation, the larger the resulting core becomes after oxidation. A more highly ordered area promotes the formation of a core shell particle for a larger particle size, but as the particle size decreases all nanocrystals show complete oxidation independently of the degree of order of the assembly. The crystalline structure of the CoO, in any nanocrystal size, is similar to that of the original fcc nanoparticles with a rather low crystallinity. The HRTEM images from the 4 and 8 nm sample are presented in the same figure (Figure 14d and 14e). From the images, the smaller nanoparticles can be detected as fully oxidized CoO with a very low crystallinity and the 8 nm nanoparticles as core/shell nanoparticles with a polycrystalline CoO shell and a core with very low crystallinity.

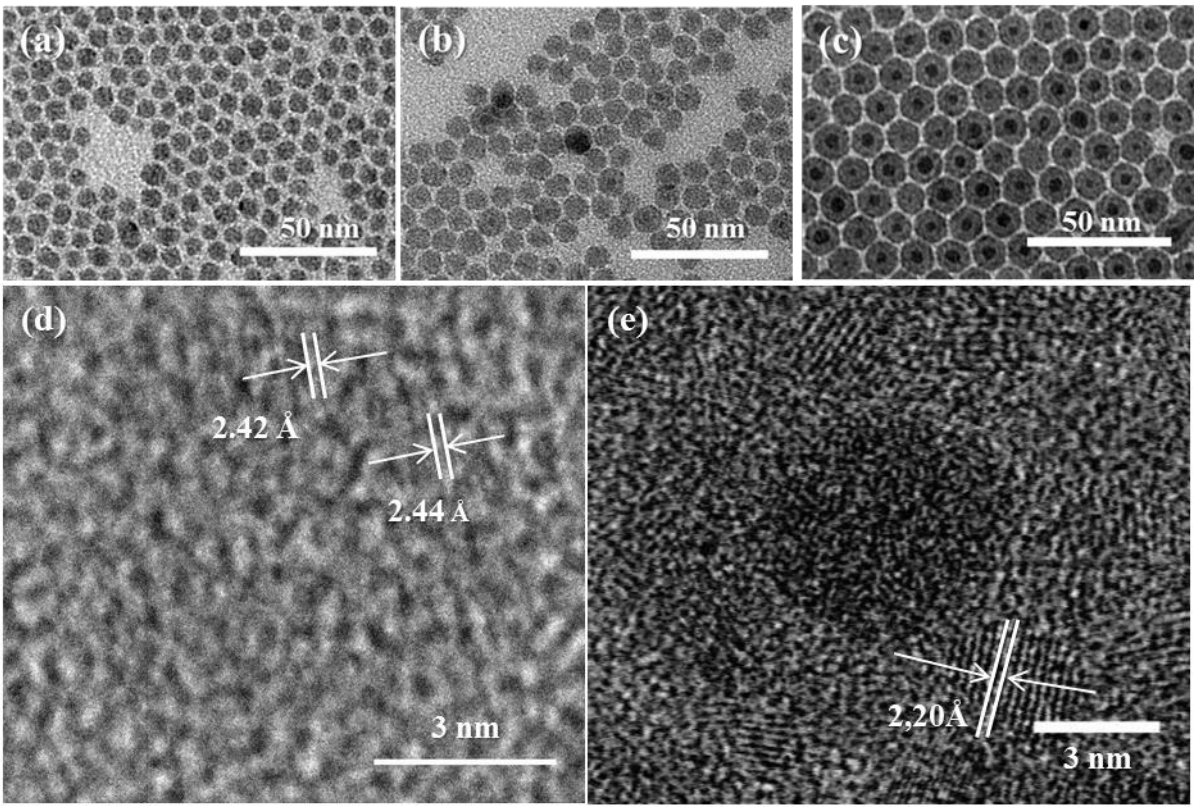

Figure 14. Polycrystalline nanocrystals produced from reverse micelles ($Co_{poly\text{-}RM}$) after oxidation at 200°C for 10 min. TEM from three different sizes and HRTEM from the sizes 4 and 8 nm, (a) TEM 4 nm, (b) TEM 6 nm, (c) TEM 8 nm, (d) HRTEM 4 nm, (e) HRTEM 8 nm.

The same comparison as described directly above is performed on the three sizes of $Co_{poly\text{-}RM}$ nanocrystals after the other investigated oxidation treatment at 260°C for 10 minutes and is presented in Figure 15. Both the TEM images and the corresponding ED pattern for the three samples are showed. The 4 nm nanoparticles have coalesced and also became fully oxidized which can be seen in

Figure 15a. The corresponding ED pattern confirms a CoO structure, but as the native $Co_{poly\text{-}RM}$ had very low crystallinity, the formed oxide has the same feature which can be seen by the unclear ED pattern. The 6 nm nanocrystals have also formed fully oxidized structures (Figure 15c) but the corresponding ED pattern (Figure 15d) reveals an uncertain oxidation state and it cannot be concluded if the oxide is the cubic CoO or the spinal Co_3O_4. One reason for this behavior can be that the 6 nm nanoparticle is in its transition state between the two oxidation states, but for a more elaborated explanation an investigation of HRTEM images would have to be made. The 8 nm nanoparticles show a mixture between fully oxidized and core/shell Co/Co_3O_4 nanoparticles (Figure 15e and 15f), the nanoparticles are slightly coalesced but it is less severe than for the smaller sizes.

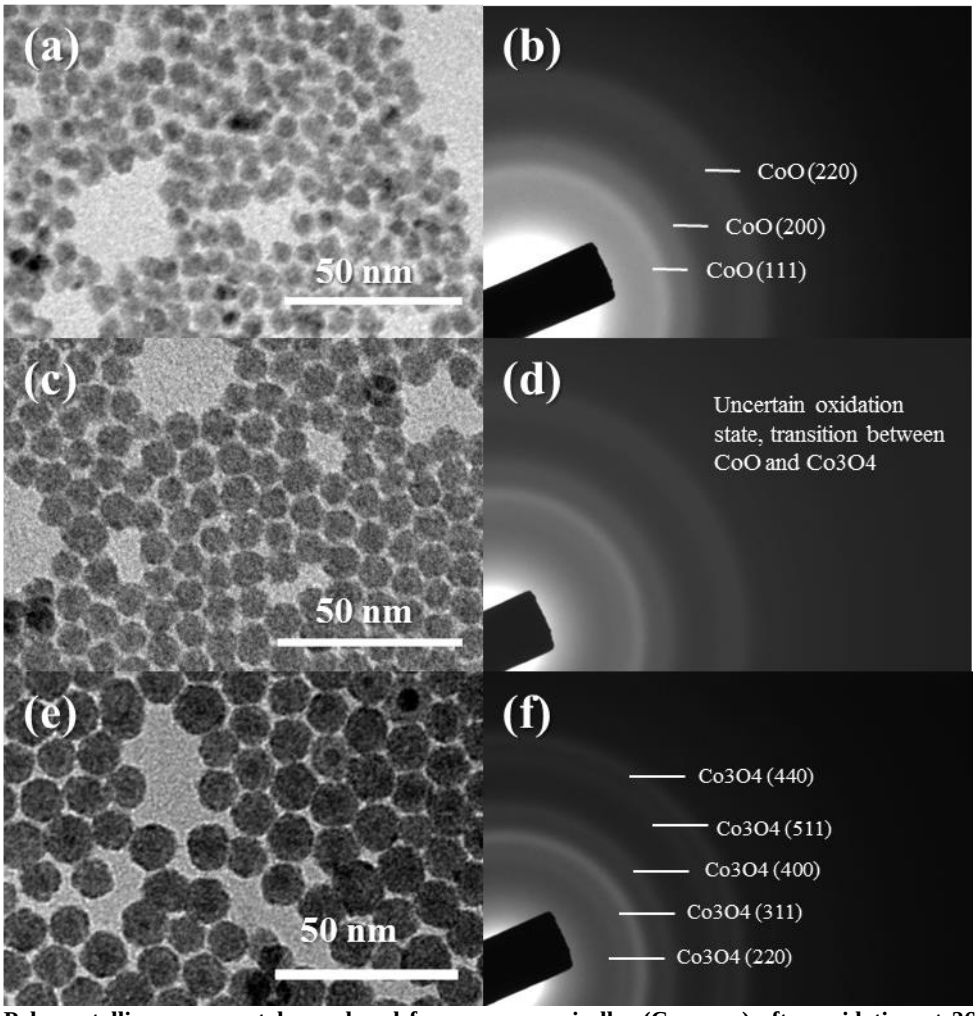

Figure 15. Polycrystalline nanocrystals produced from reverse micelles ($Co_{poly\text{-}RM}$) after oxidation at 260°C for 10 min. TEM images and ED patterns from three different sizes, (a) TEM 4 nm, (b) ED 4 nm, (c) TEM 6 nm, (d) ED 6 nm, (e) TEM 8 nm, (f) ED 8 nm.

The oxidation behavior for $Co_{poly\text{-}RM}$ has a clear size dependency. After both oxidation temperatures (200°C and 260°C) the 8 nm particles generate core/shell particles, however the oxide structure differs. When the particle size is decreased to 6 nm or below, the oxidation results in a fully oxidized structure, independently of the oxidation temperature. An interesting size dependency occurs after the oxidation at 260°C where the size of the nanoparticles affects the obtained oxide structure. The larger 8 nm nanocrystals results in the spinal Co_3O_4 and the smaller 4 nm nanocrystal in the cubic CoO structure. The 6 nm nanoparticle obtains a structure which cannot be decided to be one of the described oxides after measuring the ED pattern, and a possible solution for this could be that the 6 nm size is in its transition state in between the two possible oxide structures.

4.2.2. Single domain hcp nanocrystals produced by annealing Co nanoparticles from reverse micelle approach (Co_{HCP-RM})

A comparison between Co_{HCP-RM} nanocrystals differing by their average size before oxidation (4nm, 6nm and 8 nm) and oxidized in similar experimental conditions as above (200°C; 10mn) was performed. The resulting TEM images displays that the 4 nm Co_{HCP-RM} nanocrystals (Figure 16a) obtains a hollow single crystalline CoO structure with the HRTEM image (Figure 16d) showing the CoO (200) lattice plane.

On increasing the Co_{HCP-RM} nanocrystal size to 6 nm, hollow nanocrystals with both CoO single domain and poly crystalline phases are observed (Figure 16b, 16e and 16f). Figure 16e shows the formation of single domain hollow CoO nanocrystals with presence of the (111) planes, whereas Figure 16f shows a hollow structure with a poly crystalline CoO lattice where the CoO (200) lattice planes are oriented in different directions. The hollow void for both 4 and 6 nm is smaller than the original Co nanoparticle indicating that the diffusion mechanism is not only outward diffusion of cobalt, as this would have generated a void with equal size of the original particle. The smaller central void can be due to some inward transportation of oxygen or due to inward relaxation of the void through collection of the vacancies at the interface of cobalt and cobalt oxide. (8)

As already mentioned in chapter 4.1.2, 8 nm Co_{HCP-RM} nanocrystals are characterized by core/shell Co/CoO structure with a large core, indicating that oxidation at 200°C for 10 min is not enough to make a nanoparticle of that size into a hollow structure.

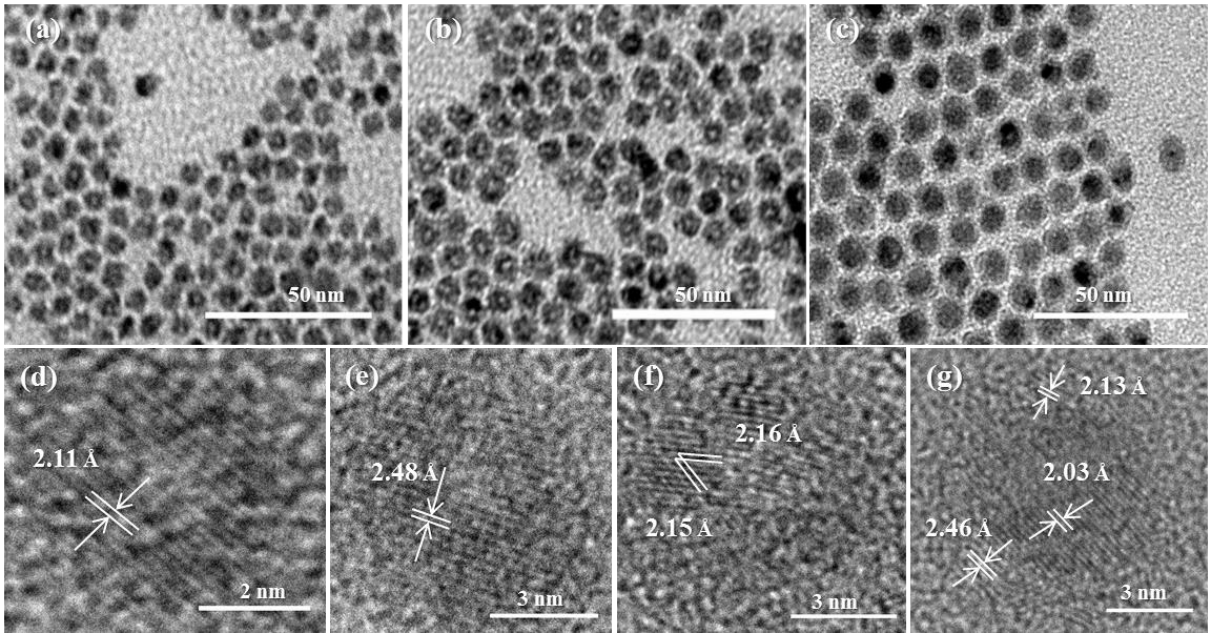

Figure 16. TEM and HRTEM images from the three different sizes of single domain hcp nanocrystals produced by annealing Co nanoparticles from reverse micelle approach (Co_{HCP-RM}) after oxidation at 200°C for 10 min. (a) TEM 4 nm nanocrystal, (b) TEM 6 nm nanocrystal, (c) TEM 8 nm nanocrystal, (d) HRTEM 4 nm, single crystalline hollow CoO particle, (e) HRTEM 6 nm, Single crystalline hollow CoO particle , (f) HRTEM 6 nm, polycrystalline hollow CoO particle, (g) HRTEM 8 nm, core/shell Co/CoO with large single crystalline core.

After increasing the oxidation temperature to 260°C for 10 minutes the particles of all the sizes have started to coalescence. The TEM image from the 4 nm nanoparticle (Figure 17a) shows fully oxidized nanocrystals. The corresponding ED pattern (Figure 17b) reveals that the oxide has the cubic CoO structure. The 6 nm nanoparticles (Figure 17c and 17d) looks fully oxidized at the first look, but as the TEM image is more carefully studies some small hollow structures can be found. According to the ED pattern the oxide structure is in this case also the cubic CoO. The TEM image and ED pattern for the 8 nm nanoparticles (Figure 17e and 17f) presents a hollow Co_3O_4 with a small void. Smaller particles have a higher surface to volume ratio and thereby a higher surface energy, this mean that a hollow

particle is less stable the smaller the particle is and could explain why the 8 nm nanoparticles result in a hollow particle while the 6 nm nanoparticles rarely presents a void and the 4 nm nanoparticles are all fully oxidized.

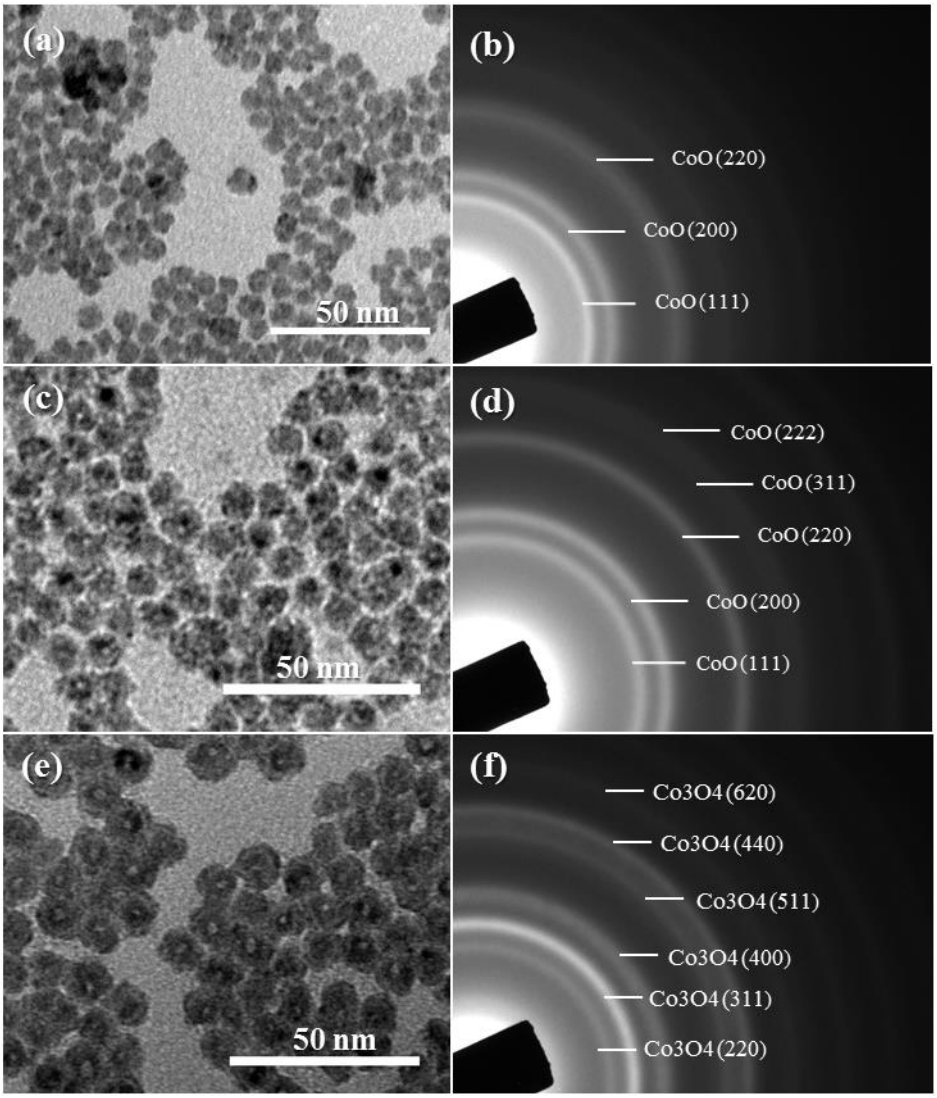

Figure 17. TEM images from three different sizes of single domain hcp nanocrystals produced by annealing Co nanoparticles from reverse micelle approach (Co_{HCP-RM}) after oxidation at 260°C for 10 min. TEM images and ED patterns from the three different sizes. (a) TEM 4 nm, (b) ED 4 nm (c) TEM 6 nm, (d) ED 6 nm, (e) TEM 8 nm, (f) ED 8 nm.

A clear size dependency can be seen among the Co_{HCP-RM} nanoparticles after both oxidation temperatures. The lower temperature (200°C) results in the same oxide structure (CoO) as the oxidation for all samples at 200°C for 10 min for all sizes however the structure of the resulting nanoparticle differs. The 4 nm nanocrystal obtains a hollow single crystalline structure while the polycrystalline structure becomes more common for the 6 nm sample. The 8 nm nanocrystal does not form a hollow nanoparticle at all but a core/shell Co_{HCP-RM}/CoO instead. The higher oxidation temperature (260°C) results in a different size dependent behavior. The larger the nanoparticle is the larger the internal central void becomes. For the 6 nm nanocrystals a void can be seen in some cases while the 4 nm nanocrystals presents a fully oxidized structure. Apart from this, the oxide structure clearly differs as well. For the two smaller sizes the oxide is built up by cubic CoO while the 8 nm nanocrystals results in the spinal Co_3O_4.

5. Conclusion

The expected result of the investigation was to find a change within the oxidation of the various single domains, between the single- and polycrystals and between the different sizes of the Co nanocrystals.

Poly- and single domain Co-nanoparticles have different oxidation behavior. Single crystalline Co-nanoparticles have a higher tendency to form hollow nanoparticles than polycrystalline Co-nanoparticles. This can be explained by the grain boundaries ability to annihilate the created vacancies without forming an internal void and thereby preventing the formation of a hollow nanoparticle in a polycrystalline structure. The grain boundaries also work as a fast diffusion track for oxygen and thereby enable the inward diffusion of oxygen to be faster than the outward diffusion of Co which hinders the formation of hollow nanocrystals. The concentration of grain boundaries are important for this behavior as the sample most near to be amorphous, polycrystalline nanocrystals produced from reverse micelles ($Co_{poly\text{-}RM}$), never showed any sign of creating a hollow particle, but the other polycrystalline sample, Polycrystalline fcc nanocrystals produced from organometallic synthesis ($Co_{poly\text{-}ORG}$), formed a yolk shell structure.

The difference in oxidation behavior is also clear between the two single crystalline and between the two poly crystalline structures. As mentioned above the concentration of grain boundaries and thereby the size of the fcc domains makes up a clear different between the two polycrystalline structures. The difference within the $Co_{poly\text{-}ORG}$ sample and the different composition if the fcc domains can be the reason for the two different results after the oxidation treatment at 200°C, the hollow CoO and the yolk/shell $Co_{poly\text{-}ORG}$/CoO. Regarding the single crystalline samples the hcp structure ($Co_{HCP\text{-}RM}$) is more stable than the ε structure ($Co_{\varepsilon\text{-}ORG}$). This means that the cobalt atoms in the ε-lattice has a higher mobility when heated and therefor an easier way for diffusion. This enables the structure to be more readily transformed into a hollow structure since the formation of a hollow structure requires the outward diffusion of Co to be faster than the inward diffusion of oxygen.

Isolated particles have in general a fast inward diffusion of oxygen as there is no protection given by surrounding particles. When particles are ordered in a 2D hexagonal network the neighboring particles slows down the rate of the inward oxygen diffusion and thereby promoted the outwards diffusion of Co. Isolated nanocrystals therefor have a higher probability of being fully oxidized than ordered nanocrystals. The oxidation behavior for the different crystal structures differ, but for all samples where isolated nanoparticles were investigated, the isolated particle was closer to being fully oxidized than the ordered nanoparticles in the same sample.

The size of the nanocrystal as well as the oxidation temperature (with a fixed oxidation time of 10 min) has an effect on which oxide (cubic CoO or spinal Co_3O_4) is obtained after oxidation. Oxidation at 200°C always generates the cubic oxide for the examined structures while the structure generated after oxidation at 260°C depends on the size and nanocrystallinity of the nanoparticle. For the single crystalline $Co_{HCP\text{-}RM}$ the spinal structure is obtained after oxidation of the 8 nm sample at the higher temperature while the cubic oxide is obtained for the 4 and 6 nm samples after the same treatment.

The higher oxidation temperature (260°C) affects the behavior differently than the lower oxidation temperature (200°C) for the smallest single crystalline $Co_{HCP\text{-}RM}$ nanoparticles. The inward relaxation seems to be made easier by the higher temperature, as the 4 nm becomes a hollow CoO for oxidation at 200°C while it becomes fully oxidized CoO after oxidation at 260°C.

5.1. Future work

Concluding the thesis will be a few suggestions for future work within the area. A more complete HRTEM study would be of interest, but as each sample takes a long time, the HRTEM images for the samples oxidized at 200°C for 10 minutes were prioritized during the project. However it would give a more detailed comparison between the two oxidation temperatures if the results were obtained for the samples oxidized at 260°C for 10 minutes as well.

References

1. **J.R. Davis.** *ASM Speciality Handbook: Nickel, Cobalt, and Their Alloys.* pp.349-406. ASM international, (2000). ISBN 0-87170-685-7.
2. **J.D. Donaldson, D. Beyersmann.** *Cobalt and Cobalt Compounds.* pp. 429-464. Ullmann's Encyclopedia of Industrial Chemistry, (2005). Vol. 9. DOI: 10.1002 14356007.
3. **H.C.Zeng.** Synthetic architechture of interior space for inorganic nanostructures. *Journal of Materials Chemistry.* 16, (2006), 649-662.
4. **Q.Zhang, J.Xie, Y.Yu, J.Yang, J.Y.Lee.** Tuningt the Crystallinity of Au Nanoparticles. *Small.* 6, (2010), 523-527. DOI: 10.1002/smll.200902033.
5. **Y.Tang, M.Ouyang.** Tailoring properties and functionalities of metal nanoparticles through crystallinity engineering. *Nature Materials.* 6, (2007), 754-759. DOI: 10.1038/nmat1982.
6. **S. Sun, C.B. Murray.** Synthesis of monodisperse cobalt nanocrystals and their assembly into magnetic superlattices (invited). *Journal of Applied physics.* 85, (1999), 4325 - 4330.
7. **Z.Yang, I.Lisiecki, M.Walls, M.P.Pileni.** Nanocrystallinity and the Ordering of Nanoparticles in Two-Dimensional Superlattices: Controlled Formation of Either Core/Shell (Co/CoO) or Hollow CoO Nanocrystals. *ACS NANO.* 7, (2013), 1342–1350. DOI: 10.1021/nn304922s.
8. **Y.D.Yin, R.M.Rioux, C.K. Erdonmez, S.Hughes, G.A.Somorjai, A.P.Alivisatos.** Formation of hollow nanocrystals through the nanoscale kirkendall effect. *Science.* 304, (2004), 711-714.
9. **F. Aldinger.** Controlled porosity by an extreme Kirkendall effect. *Acta Metallurgica.* 22, (1947), 923-928.
10. **L. Cademartiri, G.A. Ozin.** *Concepts of Nanochemistry.* Weinheim : WILEY-VCH Verlag GmbH & Co. KGaA, (2009). ISBN: 978 3 527 32597 9.
11. **H.J. Fan, U. Gösele, M. Zacharias.** Formation of Nanotubes and Hollow Nanoparticles Based on Kirkendall and Diffusion Processes: A Review. *Small.* 3, (2007), 1660-1671.
12. **V.A. de la Peña O'Shea et al.** Electronic and magnetic structure of bulk cobalt: The α, β, and ε-phases from density functional theory calculations. *The Journal of Chemical Physics.* 133, (2010), 024701(1)-(8).
13. **M. Cavalier, M. Walls, I. Lisiecki, M. P. Pileni.** How Can the Nanocrystallinity of 7 nm Spherical Co Nanoparticles Dispersed in Solution Be Improved? *Langmuir.* 27, (2011), 5014–5020. Avaliable from: dx.doi.org/10.1021/la1049887 .
14. **I. Lisiecki, M. Walls, D. Parker, M.P. Pileni.** 2D Self-Organisation of Core/Shell Cohcp/Co Nanocrystals. *Langmuir.* 24, (2008), 4295 - 4299.
15. **P.Patnaik.** *Handbook of Inorganic Chemical Compounds.* s.l. : mcgraw-Hill Professional, (2002). ISBN: 0070494398.
16. **S.C.Petitto, E.M.Marsh,G.A.Carson, M.A.Langell.** Cobalt oxide surface chemistry: The interaction of CoO(1 0 0), Co3O4 (1 1 0), and Co3O4 (1 1 1) with oxygen and water. *Journal of Molecular Catalysis A: Chemical.* 128, (2008), 49-58.
17. **J. Shi.** Steric Stabilization. *The Ohio State University.* [Online] 08 29, 2002. [Cited: 02 16, 2013.] http://www.matsceng.ohio-state.edu/ims/LR_Stericstablization.pdf.
18. **Sigma-Aldrich.** Sigma-Aldrich: Oleic Acid. [Online] 2013. [Cited: 04 25, 2013.] http://www.sigmaaldrich.com.
19. **L.E. Smart, E.A. Moore.** *SOLID STATE CHEMISTRY An Introduction.* Boca Raton : Taylor & Francis group, LLC, (2005). ISBN: 978 0 7487 7516 3.
20. **F. Krumeich.** Electron Diffraction (ED). *Electron Microscopy ETH Zürich.* [Online] 05 14, 2012. [Cited: 01 25, 2013.] http://www.microscopy.ethz.ch/ED-1.htm.